Scanning Micromirrors Fabricated by an SOI/SOI Wafer-Bonding Process

Lixia Zhou, Joseph M. Kahn, *Fellow, IEEE*, and Kristofer S. J. Pister, *Member, IEEE*

***Abstract*—MEMS scanning micromirrors have been proposed to steer a modulated laser beam in order to establish secure optical links between rapidly moving platforms. An SOI/SOI wafer-bonding process has been developed to fabricate scanning micromirrors using lateral actuation. The process is an extension of established SOI technology and can be used to fabricate stacked high-aspect-ratio structures with well-controlled thicknesses. Fabricated one-axis micromirrors scan up to 21.8° optically under a dc actuation voltage of 75.0 V, and have a resonant frequency of 3.6 kHz. Fabricated two-axis micromirrors scan up to 15.9° optically on the inner axis at 71.8 V and 13.2° on the outer axis at 71.2 V. The micromirrors are observed to be quite durable and resistant to shocks. Torsional beams with T-shaped cross sections are introduced to replace rectangular torsional beams in two-axis MEMS micromirrors, in order to reduce the cross-coupling between the two axial rotations. Fabricated bidirectional two-axis micromirrors scan up to $\pm 7°$ on the outer-axis and from $-3°$ to $7°$ on the inner-axis under dc actuation. [1524]**

***Index Terms*—Electrostatic actuation, MEMS, micromirror, silicon on insulator technology, wafer bonding.**

I. Introduction

THE convergence of MEMS technology with communication and digital circuitry makes high-speed, low power, free-space communication links over distances up to several km possible. Free-space optical communication offers significant advantages over radio frequency (RF) communication, including secure links, wide bandwidth, small terminals, low power consumption, and freedom from frequency allocation issues. Thus, optical communication is an attractive option, provided that a line-of-sight propagation path is available.

One of the key components in two-way free-space optical communication systems is a compact, reliable, and inexpensive laser beam steering device that provides a fast scanning capability for pointing, acquisition, tracking, and data communication. MEMS phased arrays composed of groups of relatively small micromirrors have been proposed to scan the laser beam [1], [2]. They can be actuated through large deflection angles with substantially reduced response time. But they involve more complicated actuator design, i.e., requiring not only rotations around the two axes, but also vertical movements to compensate the phase differences between mirrors. Also active feedback controls over individual mirrors can be very complicated. Scanning micromirror based on MEMS technology have been introduced to steer modulated laser beams between moving unmanned aerial vehicles [3], [4]. Scanning micromirrors have been developed for a wide range of other applications, such as optical crossbar switches [5], digital projectors [6], barcode readers [7], adaptive optics [8], and tunable lasers [9]. However, laser beam steering for free-space optical communication poses a somewhat unique set of requirements for micromirrors, such as large mirror sizes ($\sim 1\ \mathrm{mm}$ in diameter), rotation ability over two axes, large dc scan angles ($\pm 10°$ optical), fast switching ability (transition time between positions $< 100\ \mu\mathrm{s}$), low power consumption, and strong shock resistance (hundreds of g).

While surface micromachining generally does not offer considerable scanning range for a large mirror, MEMS micromirrors based on silicon-on-insulator (SOI) wafers and deep reactive ion etching (DRIE) technology overcome this problem by having an etched cavity under the micromirror. These fabrication technologies also offer attractive features such as excellent mirror flatness and high-aspect-ratio springs, which minimizes cross-mode coupling. Many strategies have been developed around these two technologies in order to make large-size scanning micromirrors with wide steering angles and fast scan speed. Conant *et al.* first presented a vertical comb drive actuator fabricated on the two layers of a SOI wafer [10]. However, their process requires an accurate alignment between two layers in different heights ($\sim 50\ \mu\mathrm{m}$). Consequently, several self-alignment fabrication processes were developed to enable precise alignment between vertically stacked layers [11], [12]. Other solutions to the alignment problem include using a photoresist hinge to rotate [13] or plastically displacing [14] a group of comb fingers out-of-plane so that two groups of comb fingers remain accurately spaced and form an angular comb drive actuator.

Although vertical/angular comb drive actuators provide high force density, they cannot be easily used to realize two-axis scanning micromirrors with comparable steering performance on both rotation axes. Kwon *et al.* used a backside island to provide electrical isolation and mechanical coupling for a two-axis scanning micromirror [15], but this device has a much lower resonance frequency in the outer axial rotation than that of the inner axial rotation. Milanovic *et al.* used mechanical rotation transformers to realize a two-axis scanning micromirror with high resonant frequencies [16], but obtained a limited steering range.

Scanning micromirrors realized by an off-axis lateral force overcome the alignment issue in vertical comb drive actuators,

Manuscript received February 15, 2005; revised September 14, 2005. Subject Editor C. Liu.

L. Zhou is with Qualcomm MEMS Technologies, San Jose, CA 95134 USA (e-mail: lzhou@cal.berkeley.edu).

K. S. J. Pister is with the Department of Electrical Engineering and Computer Sciences, University of California, Berkeley, CA 94727-1770 USA (e-mail: pister@eecs.berkeley.edu).

J. M. Kahn is with the Department of Electrical Engineering, Stanford University, Stanford, CA 94305-9515 USA (e-mail: jmk@ee.stanford.edu).

Digital Object Identifier 10.1109/JMEMS.2005.863736

1057-7157/$20.00 © 2006 IEEE

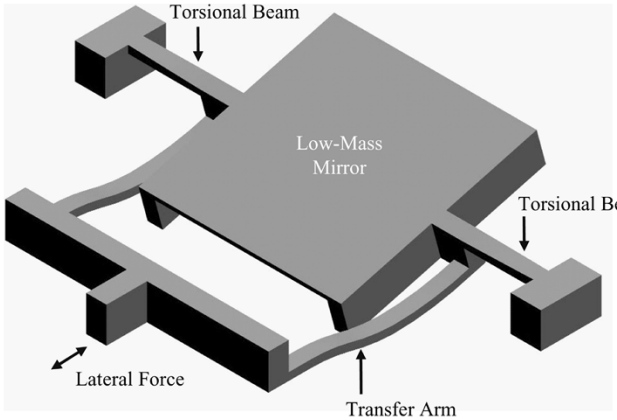

Fig. 1. Torsional movement of scanning micromirrors is realized by an off-axis lateral force generated by a lateral comb drive actuator.

and offer additional advantages, including small momentum of inertia, high actuation force, and thus large scanning angle and fast response. In this paper, we describe an SOI/SOI wafer-bonding process that can realize scanning micromirrors actuated by lateral comb drive actuators.

II. Design and Fabrication of Scanning Micromirrors Using Lateral Actuation

Our group developed the method of fabricating scanning micromirrors that utilize a lateral comb drive actuator [17]. As shown in Fig. 1, the bi-directional force generated by a lateral comb drive actuator is transferred as an off-axis torque over two torsional beams by two transfer arms.

A. Design of Scanning Micromirrors Using Lateral Actuation

An obvious benefit of this scheme is the separation of the micromirror and the actuator, which provides enhanced design flexibility. A large actuator can be designed to extend to both in-plane directions and all comb fingers always add equal amounts of moment of inertia to the device. The dc scanning range of a lateral actuated micromirror can be very large, since it is limited only by the maximum stress that the material of the device can sustain while the range of a micromirror with a vertical/angular actuator is limited by the height-to-length ratio of the comb drive finger, which is often compromised by having long fingers to provide enough torque. The lateral actuation design also offers more shock resistance as compared to a vertical comb drive actuator. The lateral movement of the device is inhibited both by the torsional beams and actuator suspension beams, in contrast to single torsional beam suspension when using a vertical comb drive actuator. The required feedback signal for controlling a micromirror can be implemented by including a group of sensing fingers directly on the electrostatic comb drive actuator [18].

B. SOI/SOI Wafer-Bonding Process

This multilevel design was formerly fabricated on an SOI wafer using a combination of timed DRIE etching and DRIE etching with etch stops. However, timed etching does not produce structures uniform across the wafer and therefore needs careful monitoring. A new approach, SOI/SOI wafer fusion bonding, is introduced to attain multilevel structures with well-controlled thicknesses.

In the proposed new process a patterned third layer is aligned and bonded onto a patterned SOI wafer, producing 3-D devices or stacked high-aspect ratio structures. The third layer comes from the device layer of another SOI wafer [19]–[21], with a choice of thickness as small as 2 μm and a thickness uniformity of ± 0.5 μm, whereas structures fabricated by the timed etching counterpart can have a thickness variation of 5 μm across a wafer. The sacrificial handle wafer of the bonded SOI wafer can be disposed of by either plasma blank etching or mechanical grinding. When the handle wafer is etched or ground to the desired thickness, a subsequent polishing step can provide another layer to the stack. Then more layers can be added by wafer fusion bonding, constructing multi-layer structures. A potential drawback of this layer stacking strategy is that bonding can become difficult as stresses in the stacked layers induce bow and warpage over the wafer. Besides stacking several levels of high-aspect-ratio structures, silicon fusion bonding introduces little or no thermal stress because of the well-matched thermal expansion between the bonded layers and the fabricated monolithic single crystal structures are completely compatible with subsequent high-temperature process steps, such as oxidation and diffusion.

Besides allowing tighter control over the thicknesses of the critical layers, potential advantages of fabricating scanning micromirrors using this new bonding process include higher yield, obtaining a functional two-axis scanning micromirror, and achievement of increased scan angles at lower actuation voltages.

C. Minimizing Bow of SOI Wafers

It has been experimentally observed that in order to achieve secure silicon-silicon bonding, the roughness of wafer surface has to be less than 1 nm and the bow of a 4-inch wafer is no greater than 5 μm [22]. Our experiments show that two wafers with a bow as large as 25 μm can be bonded reliably. However, an SOI wafer from our vendor, BCO Technologies, has a typical bow of 75 μm, preventing an adequate bonding between SOI wafers. Strategies are needed to flatten wafers and increase the yield of bonding.

The bow of an SOI wafer is mainly induced by the mismatch of thermal expansion coefficient between silicon and oxide, causing excess mechanical stresses in the SOI wafer after annealing at elevated temperatures and subsequent cooling. At high annealing temperatures, there is no internal stress between the silicon and oxide layers due to the reflow ability of the oxide layer. As temperature drops, oxide contracts but silicon shrinks more. Therefore, the thermal mismatch between silicon and oxide builds up internal stress and cause the wafer to bend. A simple model to calculate the bending caused by the thermal stress is presented in [23], considering the force balance, moment balance, and interface strain continuity for any two adjacent layers. According to this simple model, there are several ways to reduce the bow in an SOI wafer.

1) Reduce the thickness of the buried oxide layer. This idea is not practical because a certain thickness of oxide layer (preferably 2 μm) is required in order to keep the parasitic capacitance of the bonding pads and inter-connection wires small for the feedback control of mirror positions. However, a step of timed-etching the exposed oxide to a thinner thickness can be added between the DRIE etching of the device layer and the bonding of the two wafers in order to reduce the wafer stress. 10:1 HF should be used for this purpose because compared to 49% HF, its etching speed is slow enough to strictly control the remaining oxide to be thick enough for acting as the etching stop for the later DRIE etching. In this way, a thinner oxide film is left in the exposed area to reduce the stress while a 2-μm-thick oxide layer is remained under the bonding pads and interconnection wires to maintain the low parasitic capacitance.
2) Increase the thickness of the handle wafer. This is not a good solution, either, since a thicker wafer presents more difficulty in accommodating the bending and makes the bonding harder to achieve.
3) Retain an oxide layer on the backside of the handle wafer. The sandwiched structures are able to balance the stress and obtain a flatter surface. One thing to be noted is that any nonuniformity in the stress distribution might introduce warpage to the multilayered wafer. But the device layer of the SOI wafer is etched by repeating the same pattern and the thickness of the added oxide layer is uniform across the wafer. As a result, the local residual stress is expected to be minimal, and should not produce significant warpage of the wafer.

The stress-flatness model is used to find the proper oxide thickness in order to obtain the flattest wafer. For instance, the bow of the SOI wafer (with a 50-μm-thick device layer, a 2-μm -thick buried oxide layer, and a 350 μm-thick handle layer) is optimized when a 1.5-μm-thick oxide layer is added on the backside of the wafer, according to the stress-flatness model. In experiment, an unprocessed SOI wafer with the above thickness parameters was found to have a bow of 76.3 μm initially. After thermally growing a 1.5-μm-thick oxide layer on both sides of the SOI wafer and removing the front side oxide layer, the bow of the SOI wafer became 17.8 μm, which is small enough to allow a successful bonding with other SOI wafers.

D. Strategies to Enhance Bonding

Surface cleanness is another significant condition for successful wafer fusion bonding. The initial hydrogen bonding that pre-bonds two wafers are weak and operates over a short range, only when the two wafers are very close together. Therefore, having wafers flat and free with particles are critical prior to bonding.

Several steps were practiced to ensure a strong adhesion force between the two patterned SOI wafers. First, the design of the layout allocated about 50% of the wafer surface as contact area to guarantee adequate force. Second, wafers were handled carefully in the clean room. For example, a vacuum pen was used to grab a wafer on its backside whenever applicable, as particles or scratches that can destroy a bond might be introduced to the bonding surface of the wafer if using metal tweezers. Third, a layer of thermal oxide was grown on the wafers as the first step of the process and was stripped off just before cleaning and bonding occurred. This thermal oxide layer provides protection throughout the wafer handling and is a common practice to be added in the bonding process by researchers. Fourth, as suggested in the previous section, an oxide layer was retained on the backside of the SOI wafers to balance the stress introduced by the buried oxide layer in an SOI wafer. These sandwiched layers produce flatter wafers, making bonding easier. Lastly, a series of chemical cleaning steps were carried out during which a layer of hydrous thin oxide grew on the wafer surface. The hydrous oxide is highly reactive and wafers with this hydrophilic surface are ready to bond at room temperature.

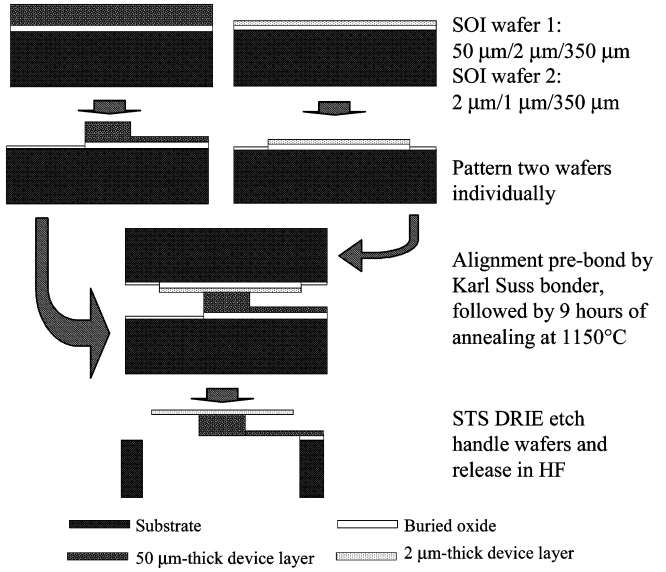

Fig. 2. Process flow for fabricating scanning micromirrors using the SOI/SOI wafer-bonding process.

E. Detailed Process Flow

As shown in Fig. 2, the process started with two SOI wafers, one with a 50-μm-thick device layer (we refer to it as the 50 μm SOI wafer) and the other with a 2 μm thick device layer (we refer to it as the 2 μm SOI wafer). First, the device layers of the two SOI wafers were patterned individually. After growing a thermal oxide layer with a thickness of 3000 Å, the device layer of the 2 μm SOI wafer was patterned with DRIE etching. For the 50-μm SOI wafer, a 1.5-μm-thick oxide layer was grown. The front side oxide is used as a mask during the later DRIE etching while the backside oxide balances the stress in the SOI wafer to achieve a flatter bonding surface. Then a timed DRIE etching step was employed to obtain a layer including nonthickness-critical structures only, such as the pushing/pulling arms for scanning micromirrors. This was done by patterning the front side oxide layer first, depositing a layer of photoresist, patterning the deposited photoresist, DRIE etching to a depth of 30 μm, peeling off the photoresist, and DRIE etching until the exposed silicon structures were 6 μm high. Keeping an oxide layer on top

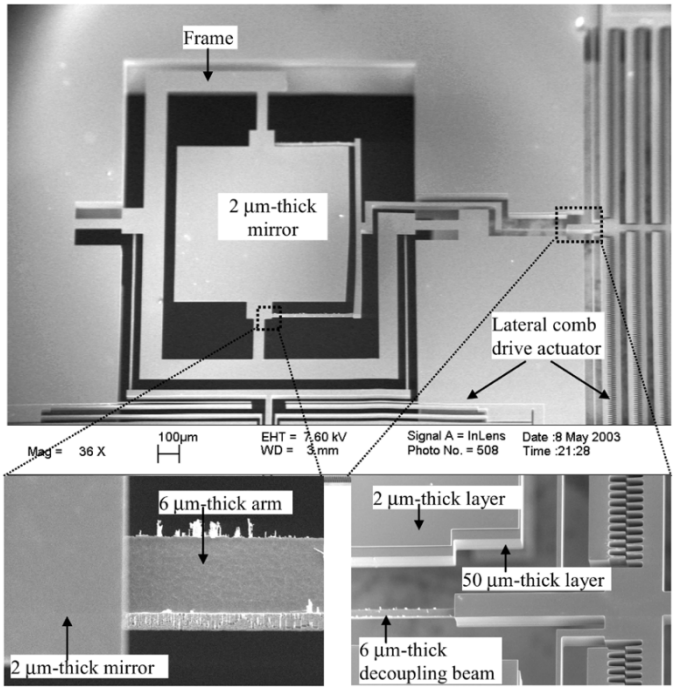

Fig. 3. Two-axis scanning micromirror fabricated by the SOI/SOI wafer-bonding process. The central mirror is suspended by two inner rectangular torsional beams and therefore rests over a rigid surrounding frame that is supported by two outer rectangular torsional beams.

of the device layer during the DRIE etching is critical for protecting the bonding surface since it is experimentally observed that the silicon surface exposed to DRIE etching does not bond. Also note that two alignment marks were patterned on the backside oxide layer of the 50 μm SOI wafer before the first DRIE etching. They are bonding alignment marks as well as the lithography alignment marks for the substrate patterning.

The next step was pre-bonding the two patterned SOI wafers with alignment and then annealing the bonded wafer pair in a furnace. After stripping off the oxide layer on the front side of the wafers in 10:1 HF, both patterned SOI wafers were cleaned in piranha, modified RCA1, RCA2 with deionized water rinsing in between. Then the two cleaned SOI wafers were aligned and pre-bonded by a Karl Suss BA6 bond aligner, followed by nine hours of annealing at 1150 °C in a furnace. An inspection using an IR microscope showed a fully bonded wafer pair.

DRIE etching was then used to dispose of the top handle wafer partially and pattern the substrate layer of the bonded wafer. With a protective layer of the top handle wafer left, the bonded wafer pair was diced into several dies. The individual dies or group of dies were DRIE etched to fully dispose of the top handle wafer afterwards. The dies were then cleaned in Piranha and released in 5:1 buffered HF. It is extremely important to clean first and release later as the HF dip before photoresist cleaning leaves polymer residues on the chip, which are extremely difficult to get rid of and often causes the electrical actuation of the micromirror to become nonfunctional. Finally the released individual chip was wire-bonded and packaged.

III. Performance of Scanning Micromirrors

A fabricated two-axis scanning micromirror is shown in Fig. 3. The micromirror is 800 μm in length and 2 μm in thickness, with 50 μm-height ribs below to stiffen the mirror. It is suspended by two 2-μm-thick, 50-μm-wide, and 200-μm-long inner torsional beams and rests over a rigid surrounding frame made up by the two bonded layers. The whole frame is then supported by two outer torsional beams that have similar dimensions as the inner torsional beams.

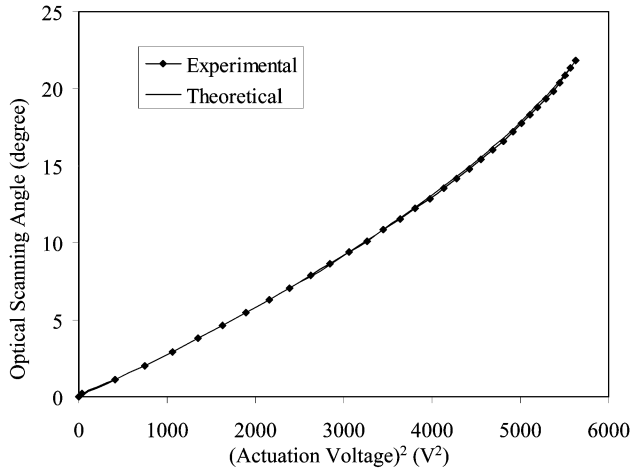

Fig. 4. DC actuation of a one-axis pulling scanning micromirror.

For both axes, there are two pushing arms connecting the torsional beams and the lateral actuator. The inner pushing arms are 6 μm in thickness, 15 μm in width, and 400 μm in length while the outer pushing arms are 6 μm in thickness, 11 μm in width, and 830 μm in length. The 6-μm-thick, 10-μm-wide, and 310-μm-long decoupling beam connecting the inner pushing arms and the inner comb drive actuator shields the actuator from rotating around the outer axis. It can be seen that the edges of 6-μm-thick beams have small silicon spikes. They are frequently seen on the structures formed by the timed DRIE etching due to the micromasking [24]. However, these grass-like defects should not affect the mechanical function of the structures since they are small in size and quantities. Fig. 3 shows only part of the two lateral comb drive actuators with tapered fingers and two of the four crab leg flexures suspending the actuator. The tapered comb fingers are designed to achieve a certain dc scanning angle at a lower actuation voltage than the one of using parallel comb fingers. As the comb fingers move in, the effective gap distance between the two groups of tapered comb fingers decreases in contrast to the constant gap distance when using parallel comb fingers. Therefore the electrostatic actuation force increases as it inversely depends on the gap distance.

A. DC and AC Actuation of Fabricated One-Axis Scanning Micromirrors

The dc response of scanning micromirrors is captured by detecting the shifts of the laser beam reflected by scanning micromirrors. Fig. 4 shows the angle displacement of a one-axis pulling-mode scanning micromirror under dc actuation. A scanning angle of 21.8° is achieved at 75.0 V with the comb drive actuator pulling in afterwards as a result of the combined effect of the side instability and rotation instability. In order to attain

a larger dc actuation range, a more stable design of the suspension beams for the comb drive actuator is required, both in terms of the side stiffness and rotating stiffness. The deviation from a linear relationship between the displaced angle and the actuation voltage is mainly due to the tapered comb fingers in the comb drive actuator. As the comb fingers are pulled closer, the gap distance between them decreases and the electrostatic force increases, inducing a larger rotation angle to the micromirror. A simple parallel-plate model of tapered comb finger actuator shows that the electrostatic force has a similar nonlinear curve as comb fingers are pulled closer. The gap between comb fingers was measured through SEM picture. The theoretical calculation of the displaced angle due to the tapered comb finger actuator is also shown in Fig. 4 and the error between theoretical curve and experimental displacement is within 1%.

Compared to the previous results reported in [25], the maximum dc scanning angle of the one-axis scanning micromirror is increased from 11.0° to 21.8°. This enhanced performance is obtained, in part, by changing the electrical connection of the device substrate from floating to ground. Leaving the substrate floating causes an uncertainty in the charge leakage and induces instability to the charge distribution on the comb drive actuator. This induces the micromirror vibrating when the actuation voltage is high. Grounding the substrate eliminates the instability of the charge distribution and the micromirror is able to work under a larger actuation voltage.

The experimental data agrees with the ANSYS analysis result. The lateral comb drive actuator is calculated to generate a pulling force of 0.97 mN at 75.0 V. The force is applied to a one-axis micromirror of similar dimensions in ANSYS and the simulation shows that the micromirror scans the laser beam up to 18.4° optically. Compared to 21.8° in experiments, the simulation result agrees with the experimental observation to be within 15%. The difference between them may arise from uncertainty in the thickness of the pushing arm, which is somewhat difficult to measure after the substrate is etched away. Typical thickness variation of the pushing arm is $\pm 20\%$. According to the analytical modeling of the mirror with the same design parameters, this translates into $\pm 30\%$ variation in the scanning angle of the mirror.

A modal analysis of the one-axis pulling mirror is carried out and calculates the first four modes of the micromirror, whose mode shapes and frequencies are shown in Fig. 5. Since the simulation only takes the mirror plate, the torsional beams, and the pulling arms into account and leaves the comb drive actuator and its suspension beams out, the mode shapes are modeled accurately while their frequencies are not modeled accurately, especially for the modes that involve large displacements of the comb drive actuator. The mode in the left, top corner of the figure corresponds to out-of-plane lateral movement of the micromirror. The mode in the right, top corner corresponds to the rotation of the micromirror. The mode in the left, bottom corner corresponds to left-right twisting motion of the micromirror. Finally, the mode in the right, bottom corner corresponds to dynamic deformation of the mirror plate. Since the out-of-plane lateral and torsion modes of the micromirror involve large displacements of the comb drive actuator in the y direction, their frequencies cannot be predicted accurately by simulation

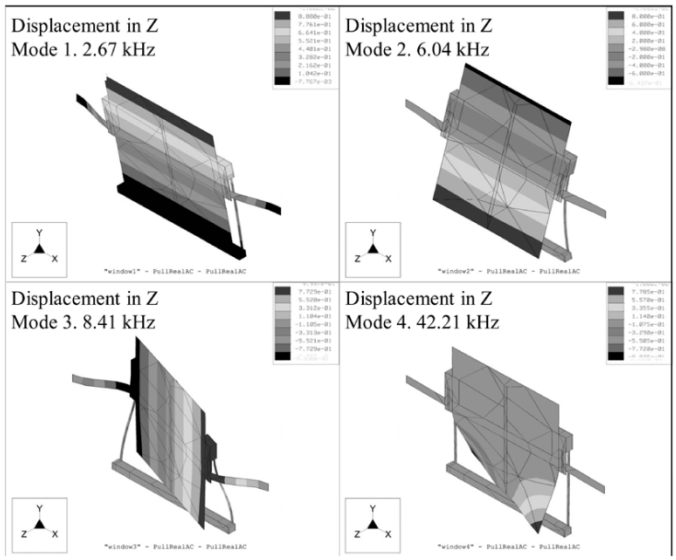

Fig. 5. Four lowest resonant mode of a one-axis pulling micromirror. Mode 1: out-of-plane lateral mode; Mode 2: rotation mode; Mode 3: left-right twisting mode; Mode 4: mirror plate deformation mode.

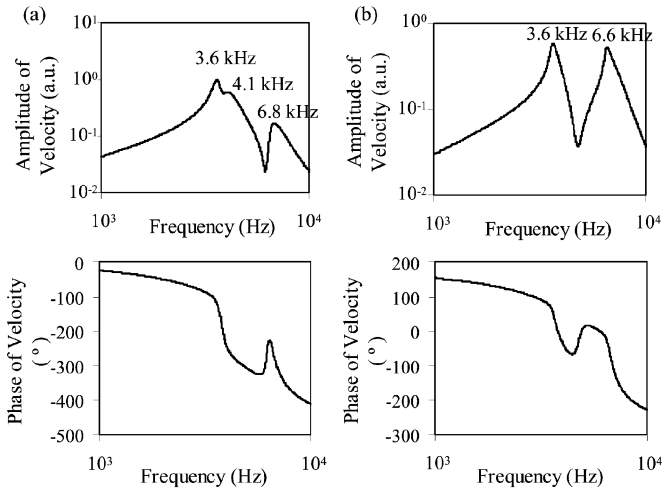

Fig. 6. Frequency response of a one-axis pulling scanning micromirror. (a) Measured on the spot where the rotation and the lateral out-of-plane mode are co-phased when actuated at low frequencies. (b) Measured on the opposite side of the mirror, where the rotation and the lateral out-of-plane modes are out-of-phase.

without including the actuator, while the frequencies of the twisting and dynamic deformation modes can be accurately predicted by simulation, given accurate device dimensions.

The ac response of the one-axis micromirror is characterized using a laser Doppler vibrometer (LDV) as the micromirror is actuated by an ac voltage source with a large dc bias. Two groups of data were taken when the laser beam from the LDV was positioned individually on the two opposite edges of the mirror, each about 400 μm from the axis of rotation. The location of the detected points is chosen so that the signal corresponding to the rotation mode of the micromirror is strongest. The amplitude and phase of the mirror movement in the out-of-plane direction are displayed in Fig. 6. Fig. 6(a) is measured on the spot where the rotation and the lateral out-of-plane mode are cophased under low frequency actuation while Fig. 6(b) is taken

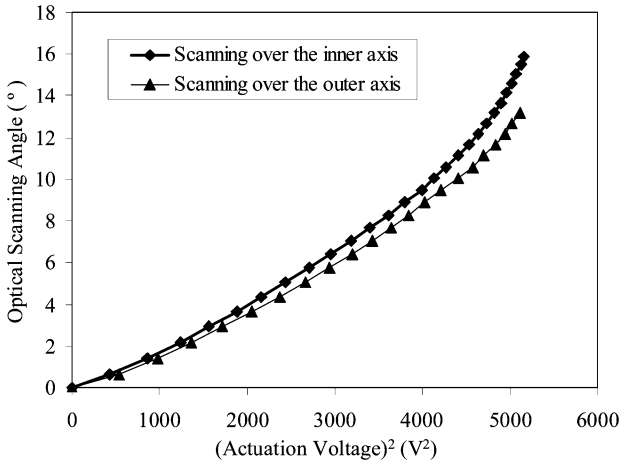

Fig. 7. DC actuation of a two-axis scanning micromirror.

on the opposite side of the mirror, where the rotation and the lateral out-of-plane modes are out of phase. The phase difference between two groups of data is 180° at most frequencies since the rotation mode dominates the movement of the mirror, except at the resonant frequencies of the out-of-plane lateral mode and left-right twisting mode. According to their phase differences, we were able to distinguish the rotational mode from the other modes. The result shows that the one-axis device has a rotational resonant frequency of 3.6 kHz with a quality factor of 12. The second mode at 4.1 kHz corresponds to the lateral out-of-plane motion of torsional beams while the additional mode at 6.8 kHz is related to the left-right twisting mode of the micromirror. Compared to the FEM simulation results of 2.67 kHz (lateral out-of-plane mode), 6.04 kHz (rotational mode), and 8.41 kHz (left-right twisting mode), the differences arise from the fact that the model does not take into account the comb drive array and its suspension beams. Furthermore, there is uncertainty in several of the dimensions used in the simulation, such as the thickness of the transfer arms.

B. DC and AC Actuation of Fabricated Two-Axis Scanning Micromirrors

The two-axis micromirror scans up to 15.9° optically on the inner axis and 13.2° on the outer axis under a static actuation, as shown in Fig. 7. The comb drive actuators pull in beyond these angles, as happened in the case of one-axis scanning micromirrors, resulting from the combined effects of the side instability and the rotation instability. Achieving a larger dc scanning range would require redesign of the suspension beams of the comb drive actuators to obtain higher stability under large displacements. There is slight cross-axis coupling between the inner and outer rotation of the two-axis micromirror. When driving the inner-axis actuator, the mirror rotates not only around the inner axis, but also the outer axis. This problem is addressed later in the paper.

The resonant frequency of the rotation mode over the inner axis for this two-axis micromirror is 2.2 kHz while the one over the outer axis is 1.3 kHz. Compared to the simulated frequencies of 2.5 kHz for the inner axis and 1.2 kHz for the outer axis, they agree within 15%.

C. Reliability and Robustness of Micromirrors

Micromirrors fabricated by the SOI/SOI wafer-bonding process are expected to be exceedingly reliable because of their monolithic single crystal silicon design. Single crystal silicon is intrinsically resistant to fatigue and the all-suspension design eliminates the frictional wear associated with contacting surfaces. Moreover, the bond formed by surface chemical-activated pre-bonding and high temperature annealing offers a high strength to hold two layers together.

However, a defective bonding interface may set off the propagation of a fatigue crack and thus the device may fail because of delamination or fracture. Also the initiation of a fatigue crack frequently occurs at the point of highest strain in the device. Therefore, the transfer arm, formed by a timed DRIE etch, may break at its linkage to the mirror plate since that point experiences the maximum stress within a whole device.

A test was carried out to assess the long-term reliability of micromirrors. A one-axis scanning micromirror was actuated for 34 days at 6.4 kHz, a frequency around its rotational resonant frequency, with scanning amplitude of 17.8° optically. The scanning micromirrors turn out to be quite durable. The change over its resonant frequency for 18.9 billion cycles is less than 1.2% and the change over the amplitude is within 2.2%. The device is still functional after operated for 18.9 billion cycles. The small and irregular change over the resonant frequency and amplitude indicates that no obvious fatigue is developed through the long-term operation of the micromirror.

The multi suspension beams with high stiffness enable the lateral-actuated micromirror to be quite resistant to shock. The acceleration of the mirror is resisted both by the torsional beams and actuator suspension beams in contrast to the single torsional beams as in the case of micromirrors with vertical/angular comb drive actuators. The high-stiffness spring design of the lateral-actuated micromirror also helps preventing the fracture or stiction of the structures under large shock loads.

A nonoperational shock test was carried out to assess the robustness of the micromirror. A 1 cm × 1 cm chip, which has one functional two-axis micromirror and two functional one-axis micromirrors, is glued onto a ceramic package using a very thin layer of silver epoxy. The package is then securely clamped on the table of a linear shake machine. We assume that this attachment mechanism does not significantly alter the shape or intensity of the shock pulse experienced by the devices. The micromirror chip was subjected to four shocks each along the directions of the x-, y-, and z-axes. Each shock, whose pulse shape was recorded by an accelerometer on the shake table, has a peak acceleration of 500 g and pulse duration of 1 ms. The devices were examined with an optical microscope as well as electrically actuated after the shock test. All three devices, including a two-axis micromirror, a pulling one-axis micromirror and a push one-axis micromirror, are still functional after the shock test.

IV. MEMS Scanning Micromirrors With T-Bar Torsional Beams

A. Torsional Beams With T-Shaped Cross Section

The previous gimbaled two-axis micromirror exhibits a cross-coupling between the two axial rotations. When a voltage is applied over the outer-axis comb drive actuator, the resulting rotation is purely around the outer axis. However, when driving the inner-axis actuator, the mirror rotates not only around the inner axis, but also the outer axis. As the voltage is increased and the mirror rotates more around the inner axis, the rotation over the outer axis increases, too.

The reason for the cross-coupling lies in the thin torsional beams of the outer gimbal with rectangular cross sections. When a lateral force pushes against the inner-axis torsional beams, the inner transfer arm bends and generates an upward force on the frame and therefore on the outer-axis torsional beams. Consequently, those two outer-axis beams bend upwards, since the 2 μm-thick torsional beams are not only susceptible to rotational motion, but also compliant to out-of-plane lateral motion. The two transfer arms attached to the outer-axis torsional beams follow the bending and produce a rotational torque onto the outer torsional beams. As a result, the mirror rotates around the outer axis.

The solution for the cross-axis coupling in the two-axis micromirror is using torsional beams that are compliant to rotational movement but robust to both in- and out-of-plane lateral movements. Torsional springs using open, thin-walled cross sections, such as T-shaped cross sections, provide such an optimal combination of spring stiffnesses [26]. Compared with a rectangular-shaped torsional beam, spring constants of T-bar torsional beams are strengthened in both lateral directions by several hundred times (depending on the dimensions of the structure) whereas the torsional stiffness is only doubled. Thus, micromirrors with T-bar torsional beams not only keep high transmission efficiency, but also have less cross-coupling between the two axial rotations.

The use of T-bar torsional beams is compatible with our current process. The web structure of the T-bar is fabricated on the 2 μm bonding layer while the flange part is made on the underlying 50 μm layer.

B. ANSYS FEM Simulation

FEM simulation confirms this analysis, as shown in Fig. 8. Fig. 8(a) shows that for a scanner with rectangular torsional beams, the torsional beams of the outer axis bend upwards and the mirror tilts around both the inner and outer axis as a pushing force, F_x, is exerted on the inner-axis transfer arm. On the contrary, in Fig. 8(b), the two-axis scanner with T-bar torsional beams shows no tilt over its outer axis and thus no cross-coupling effect between its inner and outer axes.

C. DC and AC Actuation of Micromirrors With T-Bar Torsional Beams

A fabricated two-axis scanning mirror with T-shaped cross-section torsional beams is shown in Fig. 9. The image is taken in an optical microscope using a spatial high-pass filter to show the edges clearly. As visible light is partially transmitted through a

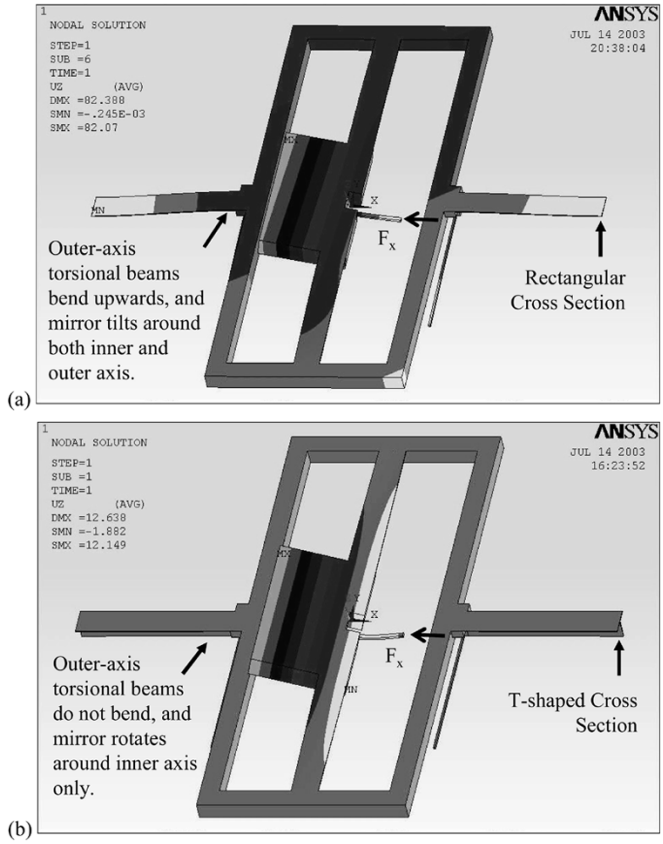

Fig. 8. (a) ANSYS simulation shows cross-coupling for two-axis scanner with rectangular shaped cross section torsional beams. (b) ANSYS simulation shows no cross-coupling for two-axis scanner with T-shaped cross section torsional beams.

2-μm silicon layer, we can see the underlying 50-μm structures. The mirror is 800 μm in diameter and 2 μm in thickness, with 50-μm-height ribs below to stiffen the mirror. The T-bar torsional beams consist of two parts, the 80 μm-wide web structure in the 2-μm-thick bonding layer and the 3-μm-wide flange part in the 50-μm-thick layer.

As stated in Fig. 10, the bidirectional two-axis micromirror works up to $\pm 7^\circ$ for the outer-axis and from -3° to 7° for the inner-axis under dc actuation. The scanner pulls in afterwards due to the same lateral and rotational instabilities in the comb drive array. The limited scanning range over the inner axis is due to a small defect on its pulling comb drive array. As predicted, there is no observed cross-coupling between two axial rotations when a two-axis micromirror rotates around its inner axis up to 15°, actuated manually with a probe.

The measured frequency response of a one-axis mirror with T-bar torsional beams using a laser Doppler vibrometer shows a torsional resonance frequency at 6.4 kHz, higher than that of a one-axis mirror with rectangular torsional beams (3.6 kHz). The second mode at 25.3 kHz is far away from the first mode, as the analytical simulation predicts.

V. Conclusions and Discussion

An SOI/SOI wafer-bonding process has been developed to fabricate scanning mirrors actuated by lateral comb drive actuators. It transfers the device layer of an SOI wafer as thin as 2 μm

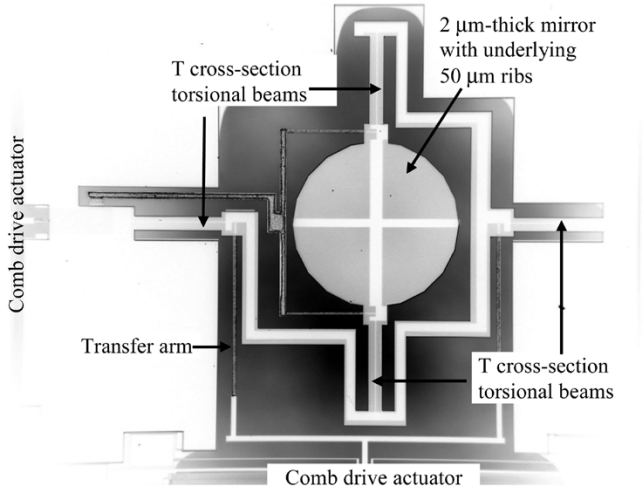

Fig. 9. Gimbaled two-axis scanner by the SOI/SOI bonding process.

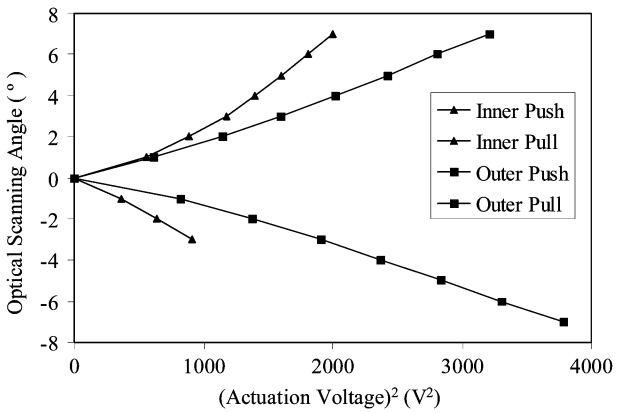

Fig. 10. DC actuation of a bidirectional two-axis scanner with T-shaped cross-section torsional beams.

onto another one and can be used to fabricate stacked high-aspect-ratio structures with well-controlled thicknesses. Strategies, such as retaining an oxide layer on the back of the SOI wafer to decrease the bow of the wafer and decreasing the thickness of the buried oxide layer to minimize the thermal stress, are employed to increase the yield of the process.

The fabricated one-axis micromirror with rectangular cross-section torsional beams has the capability of scanning 21.8° under a dc actuation voltage of 75.0 V. It agrees with the ANSYS FEM result within 15%. The frequency response of the one-axis micromirror shows that the mirror has a rotational mode at 3.6 kHz, an out-of-plane lateral mode at 4.1 kHz, and a left-right twisting mode at 6.8 kHz. The fabricated two-axis micromirror scans up to 15.9° optically under a dc actuation voltage of 71.8 V around the inner axis and 13.2° at 71.2 V around the outer axis. The resonant frequency of the rotation mode over the inner axis for this two-axis micromirror is 2.2 kHz while the one over the outer axis is 1.3 kHz.

Torsional beams with T-shaped cross sections have been introduced to replace rectangular torsional beams in the two-axis MEMS micromirror, in order to reduce the cross-coupling between the two axial rotations. T-bar torsional beams have a high lateral stiffness in both in- and out-of-plane directions while keeping a low torsional compliance. Also the use of T-bar torsional beams is compatible with the SOI/SOI wafer-bonding process used to fabricate micromirrors.

Fabricated micromirrors were observed to be quite durable, with no obvious frequency and scanning angle shifts after running at 6.4 kHz with scanning amplitude of around 17.8° for 18.9 billion cycles. There micromirrors were tested on a shake table, subjected to shocks with a peak acceleration of 500 g and pulse duration of 1 ms along the directions of all three axes. All three devices were functional after the shock tests.

Most micromirror failures are caused by pull-in of the comb drive actuators, because of their lateral and rotational instabilities under large static displacements. An ideal suspension is compliant in the direction of desired displacement and stiff in the orthogonal directions and rotations. Various strategies can be used to increase the range of dc deflections, such as increasing the width of the suspension flexure, maximizing the gap spacing of the comb drive actuator if possible, and employing pre-bent suspension beams [28] in devices that operate unidirectionally.

ACKNOWLEDGMENT

The authors acknowledge the kind support and contribution from M. Last and V. Milanovic.

REFERENCES

[1] O. Solgaard, D. Lee, Y. Kyoungsik, U. Krishnamoorthy, K. Li, and J. P. Heritage, "Microoptical phased arrays for spatial and spectral switching," *IEEE Commun. Mag.*, vol. 41, no. 3, pp. 96–102, 2003.

[2] P. B. Ruffin, "Optical MEMS-based arrays," *Proc.SPIE—The International Society for Optical Engineering*, vol. 5055, pp. 230–41, 2003.

[3] J. M. Kahn, "Secure free-space optical communication between moving platforms," in *Proc. 15th Annual Meeting of the IEEE Lasers and Electro-Optics Society*, vol. 2, 2002, pp. 455–6.

[4] M. Last, B. S. Leibowitz, B. Cagdaser, A. Jog, L. Zhou, B. Boser, and K. S. J. Pister, "Toward a wireless optical communication link between two small unmanned aerial vehicles," in *Proc. IEEE International Symposium on Circuits and Systems*, Bangkok, Thailand, 2003.

[5] D. J. Bishop, C. R. Giles, and S. R. Das, "The rise of optical switching," *Sci. Amer.*, pp. 74–9, Jan. 2001.

[6] G. A. Feather and D. W. Monk, "Digital micromirror device for projection display," *Proc. SPIE—The International Society for Optical Engineering*, vol. 2407, pp. 90–5, 1995.

[7] M. H. Kiang, O. Solgaard, R. S. Muller, and K. Y. Lau, "Micromachined polysilicon microscanners for barcode readers," *IEEE Photon. Technol. Lett.*, vol. 8, pp. 1707–9, 1996.

[8] M. A. Helmbrecht, U. Srinivasan, C. Rembe, R. T. Howe, and R. S. Muller, "Micromirrors for adaptive-optics arrays," in *Proc. 11th International Conference on Solid-State Sensors and Actuators*, vol. 2, 2001, pp. 1290–3.

[9] J. D. Berger, D. Anthon, and H. Jerman, "External cavity diode lasers tuned with silicon MEMS," *Semicond. Int.*, vol. 25, no. 2, pp. Sup18–14, 2002.

[10] R. Conant, J. Nee, K. Lau, and R. Muller, "A fast flat scanning micromirror," in *Proc. 2000 Solid-State Sensor and Actuator Workshop*, Hilton Head, SC, 2000, pp. 6–9.

[11] U. Krishnamoorthy, D. Lee, and O. Solgaard, "Self-aligned vertical electrostatic combdrives for micromirror actuation," *J. Microelectromech. Syst.*, vol. 12, pp. 458–64, 2003.

[12] V. Milanovic, S. Kwon, and L. P. Lee, "Monolithic vertical combdrive actuators for adaptive optics," in *Proc. 2002 IEEE/LEOS International Conference on Optical MEMS*, 2002, pp. 57–8.

[13] P. R. Patterson, D. Hah, H. Nguyen, H. Toshiyoshi, R. Chao, and M. C. Wu, "A scanning micromirror with angular comb drive actuation," in *Proc. 15th IEEE International Conference on Micro Electro Mechanical Systems*, 2002, pp. 544–7.

[14] J. Kim, H. Choo, L. Lin, and R. S. Muller, "Microfabricated torsional actuator using self-aligned plastic deformation," in *Proc. 12th International Conference on Solid-State Sensors and Actuators, Transducers 2003*, vol. 2, 2003, pp. 1015–8.
[15] S. Kwon, V. Milanovic, and L. P. Lee, "A high aspect ratio 2D gimbaled microscanner with large static rotation," in *Proc. 2002 IEEE/LEOS International Conference on Optical MEMS*, 2002, pp. 149–50.
[16] V. Milanovic, G. Matus, T. Cheng, and B. Cagdaser, "Monolithic high aspect ratio two-axis optical scanners in SOI," in *Proc. 2003 IEEE MEMS Conference*, 2003, pp. 255–8.
[17] V. Milanovic, M. Last, and K. S. J. Pister, "Torsional micromirrors with lateral actuators," in *Proc. 11th International Conference on Solid-State Sensors and Actuators, Transducers 2001*, Munich, Germany, 2001.
[18] B. Cagdaser, A. Jog, M. Last, B. S. Leibowitz, L. Zhou, E. Shelton, K. S. J. Pister, and B. E. Boser, "Capacitive sense feedback control for MEMS beam steering mirrors," in *Proc. 2004 Solid-State Sensor and Actuator Workshop*, Hilton Head, SC, 2004, pp. 348–51.
[19] K. Somasundram, D. Cole, C. McNamara, A. Boyle, P. McCann, C. Devine, and A. Nevin, "Fusion-bonded multilayer SOI for MEMS applications," *Proc. SPIE—The International Society for Optical Engineering*, vol. 5116, pp. 12–9, 2003.
[20] F. S. D'aragno, T. Iwamoto, H. D. Chiou, and A. Mirza, "A study of silicon direct wafer bonding for MEMS application," in *Proc. 4th International Symposium on Semiconductor Wafer Bonding: Science, Technology, and Applications*, vol. 97–36, 1998, pp. 127–37.
[21] A. Brown, G. O'Neill, and S. Blackstone, "Single-crystal micromachining using multiple fusion-bonded layers," in *Proc. SPIE—The International Society for Optical Engineering*, vol. 4174, 2000, pp. 406–15.
[22] M. Schmidt, "Wafer-to-wafer bonding for microstructure formation," *Proc. IEEE*, vol. 86, pp. 1575–85, 1998.
[23] H. C. Liu and S. P. Murarka, "Elastic and viscoelastic analysis of stress in thin films," *J. Appl. Phys.*, vol. 72, no. 8, pp. 3458–63, 1992.
[24] K. S. Chen, A. A. Ayon, X. Zhang, and S. M. Spearing, "Effect of process parameters on the surface morphology and mechanical performance of silicon structures after deep reactive ion etching (DRIE)," *J. Microelectromech. Syst.*, vol. 11, pp. 264–75, 2002.
[25] L. Zhou, M. Last, V. Milanovic, J. M. Kahn, and K. S. J. Pister, "Two-Axis scanning mirror for free-space optical communication between UAVs," in *Proc. IEEE/LEOS Optical MEMS*, HI, USA, Aug. 2003.
[26] L. Muller, A. P. Pisano, and R. T. Howe, "Microgimbal torsion beam design using open, thin-walled cross sections," *J. Microelectromech. Syst.*, vol. 10, pp. 550–60, 2001.
[27] R. Legtenberg, A. W. Groeneveld, and M. Elwenspoek, "Comb-Drive actuators for large displacements," *J. Micromech. Microeng.*, vol. 6, no. 3, pp. 320–9, 1996.
[28] J. D. Grade, H. Jerman, and T. W. Kenny, "Design of large deflection electrostatic actuators," *J. Microelectromech. Syst.*, vol. 12, pp. 335–43, 2003.

Lixia Zhou received the B.S. degree in applied physics and the B.E. degree in computer science and technology from Tsinghua University in 1996. She received the M.S. and Ph.D. degrees in electrical engineering and computer science from the University of California at Berkeley in 2002 and 2004, respectively.

She is currently with Qualcomm MEMS Technologies, San Jose, CA, where she is working on the research and development of iMod (interferometric modulation) displays, based on a microelectromechanical systems (MEMS) structure combined with thin-film optics.

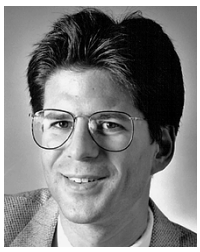

Joseph M. Kahn (M'90–SM'98–F'00) received the A.B., M.A., and Ph.D. degrees in physics from the University of California at Berkeley in 1981, 1983, and 1986, respectively.

He is currently a Professor in the Department of Electrical Engineering at Stanford University, Stanford, CA. Previously, he was a Professor in the Department of Electrical Engineering and Computer Sciences at University of California at Berkeley. In 2000, he co-founded StrataLight Communications, Inc., where he is currently Chief Scientist. From 1987 to 1990, he was a Member of Technical Staff in the Lightwave Communications Research Department of AT&T Bell Laboratories, where he performed research on multigigabit per second coherent optical fiber transmission systems, setting world records for receiver sensitivity. His current research interests include optical fiber communication, free-space optical communication, and wireless communication for sensor networks based on microelectromechanical systems.

Prof. Kahn received the National Science Foundation Presidential Young Investigator Award in 1991. He is a Member of the IEEE Communications Society and the IEEE Lasers and Electro-Optics Society. From 1993 to 2000, he served as a Technical Editor of IEEE PERSONAL COMMUNICATIONS MAGAZINE.

Kristofer S. J. Pister (M'03) received the B.A. degree in applied physics from the University of California, San Diego (UCSD), in 1986 and the M.S. and Ph.D. degrees in electrical engineering from University of California, Berkeley (UC Berkeley), in 1989 and 1992, respectively.

From 1992 to 1997, he was an Assistant Professor of Electrical Engineering at the University of California, Los Angeles (UCLA), where he helped developed the graduate MEMS curriculum, and coined the phrase Smart Dust. Since 1996, he has been a Professor of Electrical Engineering and Computer Sciences at UC Berkeley. In 2003 and 2004, he was on leave from UC Berkeley as CEO and then CTO of Dust Networks, a company he founded to commercialize wireless sensor networks. He has participated in many government science and technology programs, including the DARPA ISAT and Defense Science Study Groups, and he is currently a member of the Jasons. His research interests include micro robotics, sensor networks, and low-power circuits.